Antiferromagnetic ordering and crystal-field splittings of the Ho^{3+} ions in $HoBa_2Cu_4O_8$

1994 J. Phys.: Condens. Matter 6 4147

(http://iopscience.iop.org/0953-8984/6/22/014)

J. Phys.: Condens. Matter 6 (1994) 4147–4152. Printed in the UK

Antiferromagnetic ordering and crystal-field splittings of the Ho^{3+} ions in $HoBa_2Cu_4O_8$

B Roessli†, P Fischer†, M Guillaume†, J Mesot†, U Staub†, M Zolliker†, A Furrer†, E Kaldis‡, J Karpinski‡ and E Jilek‡

† Laboratorium für Neutronenstreuung, Eidgenössische Technische Hochschule Zürich and Paul Scherrer Institut, CH-5232 Villigen PSI, Switzerland

‡ Laboratorium für Festkörperphysik, ETH Zürich, CH-8093 Zürich, Switzerland

Received 9 March 1994

Abstract. The antiferromagnetic structure of the high-temperature superconductor $HoBa_2Cu_4O_8$ with $T_c = 77$ K was determined by means of neutron diffraction at $T = 9$ mK. Imperfect three-dimensional antiferromagnetic ordering of the Ho^{3+} ions corresponding to propagation vector $K = [0, \frac{1}{2}, 0]$ is found below $T_N = 100$ mK with magnetic moments of magnitude 1.5 μ_B at saturation and oriented parallel to the a-axis. The antiferromagnetic sublattice is characterized by stacking faults corresponding to a finite correlation length $\xi_c = 18$ Å along the c-axis. The majority of the 17 crystal-field levels within the ground-state J-multiplet of the Ho^{3+} ions is established by inelastic neutron scattering, which allowed an unambiguous determination of the nine assignable crystal-field parameters. The observed temperature dependence of the order parameter is found to be in excellent agreement with mean-field calculations including crystal-field, exchange and hyperfine interactions.

1. Introduction

The 80 K superconductors $RB_2Cu_4O_8$ (R = yttrium or rare earth) have double CuO chains in the unit cell instead of the single CuO chain characteristic of the $RBa_2Cu_3O_x$ ($6 \leqslant x \leqslant 7$) compounds. Due to the *Ammm* symmetry of the chemical cell, the rare-earth sublattice is face centred and contains two R ions in the unit cell shifted by $(b+c)/2$. The large separation of nearest-neighbour rare-earth ions along the c-axis ($c \simeq 27$ Å) renders the magnetic characteristics highly anisotropic and favours two-dimensional (2D) magnetic ordering. In fact, neutron-diffraction experiments in $DyBa_2Cu_4O_8$ revealed 2D antiferromagnetic ordering with propagation vector $K = [\frac{1}{2}, \frac{1}{2}]$ at temperatures as low as 7 mK and an Ising temperature dependence of the magnetic order parameter [1]. On the other hand, 3D antiferromagnetic ordering was found in $ErBa_2Cu_4O_8$ with propagation vector $K = [0, \frac{1}{2}, 1]$ below $T_N = 0.49$ K [2].

In previous papers we showed that 3D antiferromagnetic ordering in $HoBa_2Cu_3O_x$ ($x = 7.0$, 6.8) is imperfect and driven by a combined nuclear–electronic mechanism, i.e. polarization effects through the spins of the nuclei have to be invoked to achieve antiferromagnetic ordering at low temperatures [3]. In this paper we report on neutron-scattering experiments performed in polycrystalline $HoBa_2Cu_4O_8$. The magnetic structure was investigated by neutron diffraction at 9 mK, and the crystal-field level scheme was determined for the same sample by neutron spectroscopy. The temperature dependence of the sublattice magnetization is interpreted in terms of a mean-field model including crystal-field, exchange and hyperfine interactions.

0953-8984/94/224147+06$19.50

2. Experiments

The $HoBa_2Cu_4O_8$ sample was synthesized by means of a high-oxygen-pressure technique. The same sample has previously been used for high-resolution neutron-diffraction experiments [4]. The neutron-diffraction measurements were performed on the multi-counter DMC diffractometer at the Saphir reactor of the Paul Scherrer Institut at Würenlingen (Switzerland) operating in the high-intensity mode (vertically focusing Ge (311) monochromator, wavelength 1.7036 Å, without primary collimator). An oscillating collimator placed between the sample and the detector (opening 12') was used to suppress the scattering from the cryostat. The sample was enclosed in a cylindrical Cu container (10 mm diameter, 50 mm height) and mounted inside a bottom-loading ^{3,4}He dilution refrigerator attaining 9 mK. To achieve good thermal contact ^{4}He was condensed into the sample voids. The raw data were corrected for absorption according to the measured transmission.

The inelastic neutron-scattering experiments were performed at the Saphir reactor on the MARC triple-axis spectrometer operated in the neutron energy-loss configuration. The energy of the scattered neutrons was kept fixed either at 5 meV or 15 meV. The sample was enclosed in a cylindrical Al container (10 mm diameter, 40 mm height) and mounted in an orange ILL-type He cryostat. Some additional experiments have been carried out at the ILL Grenoble (IN4) (time-of-flight spectrometer) and at the RAL Didcot (MARI spectrometer).

3. The antiferromagnetic structure of $HoBa_2Cu_4O_8$

The magnetic part of the cross section for neutron diffraction from magnetic samples with polarized nuclei and unpolarized neutrons is given by [5]

$$\sigma/4\pi = A^2 M_\perp^2 + 2Ab_N I M_\perp \cdot P + b_N^2 I^2 P^2 \tag{1}$$

where $A = 0.2696 \times 10^{-12}$ cm is the electronic magnetic scattering length. $M_\perp \equiv M_\perp(Q) = M(Q) - [\hat{Q} \cdot M(Q)]\hat{Q}$ with $M(Q) = g_J f(Q) J$ is the component of the magnetization perpendicular to the scattering vector Q and J is the total angular momentum. $f(Q)$ is the electronic form factor and P denotes the polarization vector of the nuclei. b_N is the scattering length of a thermal neutron by a nuclear spin I and may by modelled by attributing to the nucleus a pseudonuclear moment $\mu^*/\mu_B = b_N I/r_0 g = -0.555$, with $r_0 = 2.8179$ fm and $g = -1.9132$ [6]. We assumed antiparallel polarization of the ^{165}Ho nuclei with respect to the (induced) Ho electronic moments, similar to $HoBa_2Cu_3O_x$ [3]. The least-squares refinements of the observed magnetic diffraction patterns were carried out by means of a modified version of the program MINREF [7] including instrumental resolution and using (1). The electronic form factor of Ho^{3+} was used in the relativistic dipole approximation [8].

Figure 1(a) shows the magnetic diffraction pattern of $HoBa_2Cu_4O_8$ measured at $T = 9$ mK. The nuclear contribution was eliminated from the diffraction pattern by calculating the difference for $T = 9$ mK and $T = 400$ mK. The antiferromagnetic structure of $HoBa_2Cu_4O_8$ corresponds to the propagation vector $K = [0, \frac{1}{2}, 0]$, as the magnetic peaks can be indexed by the Miller indices $(0, \frac{1}{2}, 0)$, $(0, \frac{1}{2}, 1)$, $(0, \frac{1}{2}, 2)$, ... with increasing scattering angle 2θ. Therefore, the magnetic unit cell of $HoBa_2Cu_4O_8$ is doubled along the b crystallographic direction with respect to the chemical one. The Ho^{3+} antiferromagnetic structure is shown in figure 2. Figure 3 shows the temperature dependence of the observed neutron intensities for the $(0, \frac{1}{2}, 0)$ magnetic reflection yielding the Néel temperature $T_N = (100 \pm 5)$ mK.

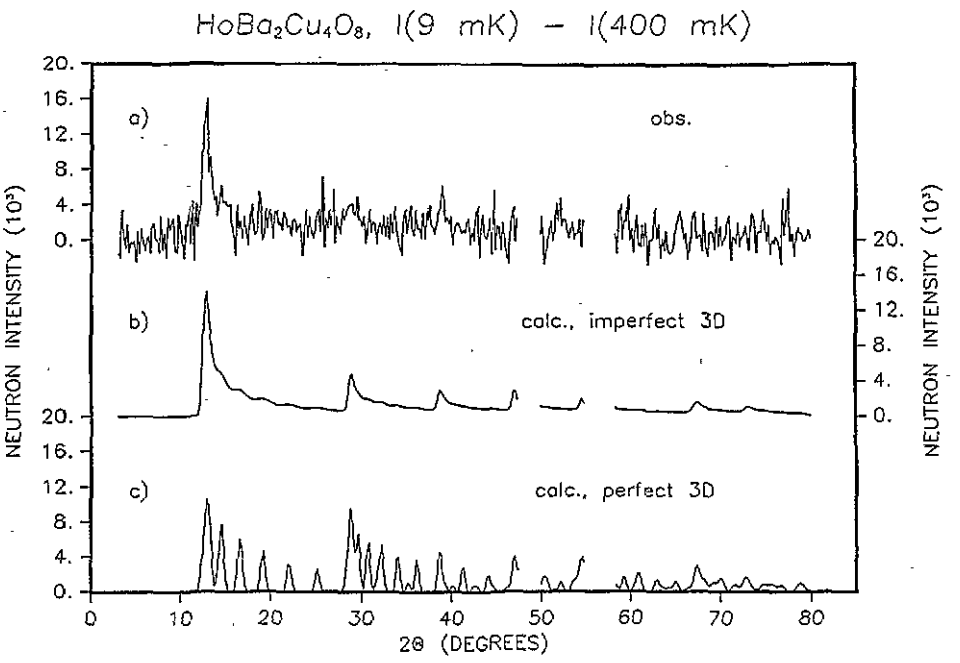

Figure 1. (a) The magnetic neutron diffraction pattern [I(9 mK) $-I$(400 mK)] of $HoBa_2Cu_4O_8$. The background is subtracted from the data. The scattering angles corresponding to the Cu reflections of the sample container are excluded from the diffraction pattern. (b) The calculated neutron-diffraction pattern of $HoBa_2Cu_4O_8$ corresponding to propagation vector $\boldsymbol{K} = [0, \frac{1}{2}, 0]$ and finite correlation length ξ_c = 18 Å, as explained in the text. (c) The calculated neutron diffraction pattern of $HoBa_2Cu_4O_8$ corresponding to propagation vector $\boldsymbol{K} = [0, \frac{1}{2}, 0]$ and infinite correlation length, as explained in the text.

Analogous to the case of $HoBa_2Cu_3O_x$ [3], the unusual line shapes observed in the magnetic neutron diffraction pattern of $HoBa_2Cu_4O_8$ can be shown to result from finite magnetic correlations along the c-axis, which is equivalent to the occurrence of magnetic stacking faults along that direction. Assuming a Poisson distribution of the magnetic correlation lengths along the c-axis results in a Lorentzian-shaped magnetic density in Fourier space of every reflection (h, k, l) [9]:

$$I_{hkl}(\boldsymbol{q}) \propto \left[\Gamma/\pi\left(\Gamma^2 + |\tau_{hkl} - \boldsymbol{Q}|^2\right)\right]\delta(q_a)\delta(q_b) \tag{2}$$

with $\boldsymbol{q} = (q_a, q_b, q_c) = \tau_{hkl} - \boldsymbol{Q}$. τ_{hkl} is a reciprocal lattice vector.

Figure 1(b) represents the result of a least-squares procedure for the measured data by convoluting (1) and (2) with the known spectrometer resolution function and using the Laue theorem for diffraction from polycrystalline samples. The calculation yields a finite correlation length between the magnetic Ho^{3+} ions along the c-axis $\xi_c = (18 \pm 3)$ Å and the easy direction of the magnetic moments parallel to the a-axis. By scaling the magnetic diffraction pattern with the nuclear peaks we obtain the magnetic moment value $\mu_{Ho} = (1.5 \pm 0.4)\ \mu_B$. For comparison we also show in figure 1(c) the result of the calculation assuming infinite correlation lengths along the three crystallographic directions $\xi_a = \xi_b = \xi_c = \infty$, yielding a much poorer agreement with the measured data.

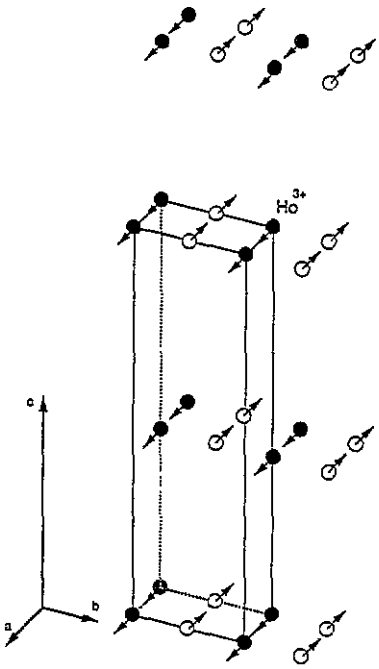

Figure 2. The antiferromagnetic structure of $HoBa_2Cu_4O_8$ below T_N = 100 mK. The arrows denote the Ho^{3+} magnetic-moment directions.

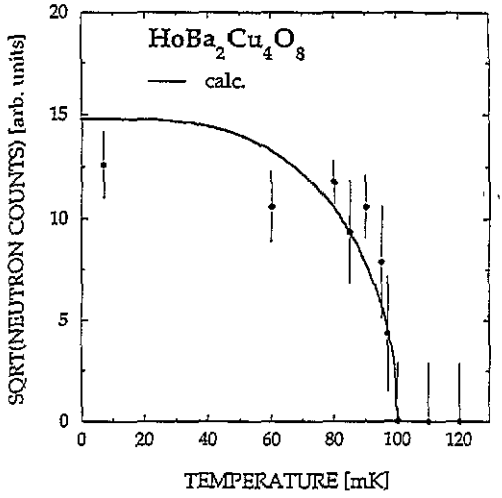

Figure 3. The temperature dependence of the square root of the $(0, \frac{1}{2}, 0)$ magnetic reflection. The line is the result of the calculations explained in the text.

4. Inelastic neutron-scattering analysis of crystal-field levels in $HoBa_2Cu_4O_8$

The crystal-field Hamiltonian for the orthorhombic symmetry D_{2h} of the Ho^{3+} ions is given by

$$H_{CF} = \sum_{n=1}^{3} \sum_{m=0}^{n} B_{2n}^{2m} O_{2n}^{2m} \tag{3}$$

where the B_{2n}^{2m} denote the crystal-field parameters and the O_{2n}^{2m} are operator equivalents built up by spin operators. (3) completely lifts the 17-fold-degenerate ground-state multiplet $^5I_8$ of the Ho^{3+} ions into 17 singlets ($5 \times \Gamma_1$, $4 \times \Gamma_2$, $4 \times \Gamma_3$, $4 \times \Gamma_4$). Typical energy spectra are shown in figure 4. The crystal-field splitting of $HoBa_2Cu_4O_8$ turns out to be very similar to the case of $HoBa_2Cu_3O_x$ [10, 11]. We can immediately interpret all the inelastic lines in terms of crystal-field transitions out of the ground state, since none of the excited crystal-field states are sufficiently populated below 2 K. Thus we have been able to observe the energies and intensities of ten among the thirteen allowed ground-state transitions, which is sufficient to determine the nine independent crystal-field parameters of the Hamiltonian (3). The procedure adopted in the least-squares data refinement was the same as described for $HoBa_2Cu_3O_x$ [10]. Good agreement between observed and calculated energies and intensities was obtained for the following crystal-field parameters:

$$B_2^0 = (-0.55 \pm 0.08) \times 10^{-1} \text{ meV}$$

$$B_2^2 = (-0.14 \pm 0.02) \times 10^{-1} \text{ meV}$$

$$B_4^0 = (0.91 \pm 0.01) \times 10^{-3} \text{ meV}$$

$$B_4^2 = (0.0 \pm 0.5) \times 10^{-3} \text{ meV}$$

$$B_4^4 = (-0.44 \pm 0.01) \times 10^{-2} \text{ meV}$$

$$B_6^0 = (-0.432 \pm 0.005) \times 10^{-5} \text{ meV}$$

$$B_6^2 = (0.4 \pm 0.3) \times 10^{-5} \text{ meV}$$

$$B_6^4 = (-0.135 \pm 0.001) \times 10^{-3} \text{ meV}$$

$$B_6^6 = (0.1 \pm 0.3) \times 10^{-5} \text{ meV}$$

More detailed information on the neutron spectroscopic study of the crystal-field splitting in $HoBa_2Cu_4O_8$ will be published elsewhere [12].

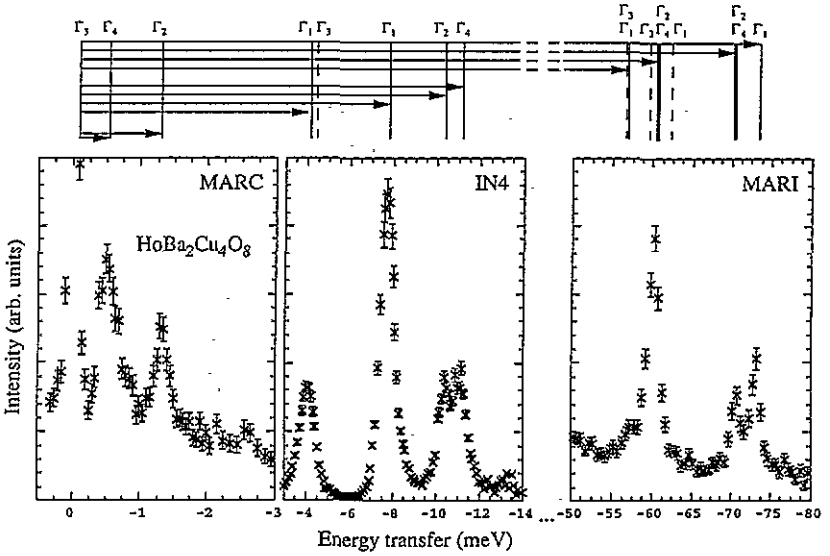

Figure 4. Energy spectra of neutrons scattered from $HoBa_2Cu_4O_8$ at 2 K. The upper part of the figure shows the resulting crystal-field energy-level scheme. The arrows denote the observed transitions.

5. Discussion and concluding remarks

The magnetic single-ion susceptibility calculated from the crystal-field results yields the *a*-axis as the easy axis of magnetization, in agreement with the magnetic structure determined by neutron diffraction. The interpretation of the temperature dependence of the intensities observed by neutron diffraction is based on a Hamiltonian that includes crystal-field (3), exchange and hyperfine interactions:

$$H = H_{CF} - \lambda \langle J_x \rangle J_x + a J_x I_x. \tag{4}$$

a = 39 mK is the hyperfine coupling constant as determined by EPR measurements [13], and x is the easy axis of magnetization. The only adjustable parameter is the molecular-field constant λ which has been chosen such as to correctly predict the Néel temperature T_N = 100 mK. We find λ = 64 mK. Figure 3 shows the results of our calculations for the scattered intensity, based on (1) and (4) and taking into account the full crystal-field energy-level scheme on $HoBa_2Cu_4O_8$ as measured by neutron spectroscopy in the present work. At T = 9 mK the calculated magnetic moment turns out to be $\mu = 1.82\mu_B$, which compares nicely to the measured value $\mu = (1.5\pm0.4)\mu_B$.

In conclusion, we have shown that the magnetic ordering of the Ho^{3+} ions in $HoBa_2Cu_4O_8$ below T_N = 100 mK is very similar to that in the compound $HoBa_2Cu_3O_x$ (x = 7.0, 6.8) with imperfect 3D ordering and polarized nuclei. The small correlation length $\xi_c \simeq$ 18 Å is smaller than the lattice parameter $c \simeq$ 27 Å, so that less than three magnetic ions are coupled along the c-axis, similar to $Dy_2Ba_4Cu_7O_{15}$, where the magnetic diffraction pattern could be explained by considering 2D antiferromagnetic ordering with ferromagnetically coupled bilayers along the c-axis [14].

Acknowledgments

This work was partly supported by the Swiss National Science Foundation. The authors are indebted to S Fischer for expert technical assistance in the dilution refrigerator experiments. The collaboration of Z Bowden, A Taylor and H Mutka in some of the experiments is gratefully acknowledged.

References

[1] Roessli B, Fischer P, Zolliker M, Allenspach P, Mesot J, Staub U, Furrer A, Kaldis E, Bucher B, Karpinski J and Jilek E 1993 *Z. Phys.* B **91** 149
[2] Zhang H, Lynn J W, Li W H, Clinton T W and Morris D E 1990 *Phys. Rev.* B **41** 11 229
[3] Roessli B, Fischer P, Staub U, Zolliker M and Furrer A 1993 *Europhys. Lett.* **23** 511; *J. Appl. Phys.* at press
[4] Fischer P, Roessli B, Mesot J, Allenspach P, Staub U, Kaldis E, Bucher B, Karpinski J, Rusiecki J, Jilek E and Hewat A W 1992 *Physica* B **180 & 181** 414
[5] Brown P J, Forsyth J B, Hansen P C, Leask M J M, Ward R C C and Wells M R 1990 *J. Phys.: Condens. Matter* **2** 4471
[6] Glättli H and Goldman M 1987 *Methods Exp. Phys.* **23** 262
[7] Elsenhans O 1990 *J. Appl. Crystallogr.* **23** 73
[8] Freeman A J and Desclaux J P 1990 *J. Magn. Magn. Mater.* **12** 11
[9] Goldman M 1980 *J. Physique* **41** 885
[10] Furrer A, Brüesch P and Untermährer P 1988 *Phys. Rev.* B **38** 4616
[11] Staub U, Allenspach P, Mesot J, Furrer A, Blank H and Mutka H 1992 *Physica* B **180 & 181** 417
[12] Staub U, Guillaume M, Mesot J, Furrer A, Bowden Z, Taylor A and Mutka H to be published
[13] Abragam A and Bleaney B 1970 *Electron Paramagnetic Resonance of Transition Ions* (Oxford: Clarendon)
[14] Zhang H, Lynn J W and Morris D E 1992 *Phys. Rev.* B **45** 10 022